Optica Applicata, Vol. XLV, No. 4, 2015
DOI: 10.5277/oa150410

Predicting emission spectra of fluorescent materials from their absorbance spectra using the artificial neural network

A. SHAMS-NATERI[1, 2*], N. PIRI[1]

[1]Textile Engineering Department, University of Guilan, Rasht, Iran

[2]Center of Excellence for Color Science and Technology, Tehran, Iran

[*]Corresponding author: a_shams@guilan.ac.ir

Artificial neural networks have been shown to be able to approximate any continuous nonlinear functions and have been used to build data based empirical models for nonlinear processes. This work studies primarily the performance of neural networks as a tool for predicting the emission spectra of fluorescent materials from their absorbance, and further, tends to the determination of the optimal topology of the neural network for this purpose. In order to do this, spectral data were initially analyzed by a principal component analysis technique. The first four principal components were used as input nodes of neural networks with various training algorithms – namely cascade- and feed-forward algorithms – and also, various numbers of hidden layers and nodes. The obtained results indicate that the RMS error in a testing data set decreased with increasing the number of neurons and the minimal network architecture for a data prediction problem consists of two hidden layers, respectively with 9 and 1 nodes for both neural networks. Additionally, a better performance was obtained with the cascade-forward neural network, especially in a small number of nodes. The obtained results indicate that the neural networks can be used to provide a relationship between the absorbance as an input and the emission as a target.

Keywords: fluorescence, prediction, absorbance, emission, neural networks.

1. Introduction

Fluorescence typically occurs from aromatic molecules. Fluorescent chromophores have been generally known to have planar and rigid π-conjugation systems, and many fluorescent chromophores have rigid ring systems including stilbene, coumarin, naphthalimide, perylene, rhodamine and other structures [1–6]. Fluorophores are also denoted as chromophores, historically speaking the part or moiety of a molecule responsible for its color. Most known stable and bright fluorophores absorb and emit in the wavelength range between 300 and 700 nm [7]. The most dramatic aspect of fluorescence is its occurrence at wavelengths longer than those at which absorption occurs. Fluorescence spectral data are generally presented as emission spectra. A fluorescence emission spectrum is a plot of the fluorescence intensity *versus* wavelength (nm) or

wave number (cm^{-1}). Emission spectra vary widely and are dependent upon the chemical structure of the fluorophore and the solvent in which it is dissolved [8].

Over the recent years, the development of fluorescent molecules has been progressing remarkably due to their potential applications and many fluorophores have been synthesized and utilized in fields as diverse as fluorescent dyes, sensors and solar cells. Fluorescent proteins also are now a critical tool in all areas of biomedical research and play the central role in fluorescence spectroscopy [9–15].

Principal component analysis (PCA) technique has been an important and useful mathematical tool in color science and technology. In color technology, PCA is mainly used for data compression, dimensionality reduction and also to define the principal directions that a set of data orients. As dominant sample variations are along several significant directions, data reduction could be accomplished by neglecting the unimportant directions. The number of these directions approximates the dimensionality of the sample set. Each reconstructed reflectance spectrum R_c can be represented through the sum of the small number m of basic functions PC_j as shown in the following equation:

$$R_c = R_0 + \sum_{j=1}^{m} C_j \mathrm{PC}_j \tag{1}$$

where C_j is the weight of the j-th basis function and R_0 shows the mean spectral reflectance of the data set.

Neural networks have been successfully developed to solve problems in textile industry in a variety of applied fields from environment to textile defects and color constancy [16–21].

Although neural networks are an established tool, their optimization remains a matter of active research. Several researches have been dealt with determination of the optimal topology of a neural network for specific applications [22–24].

Artificial neural networks may be constructed in a variety of sizes and with different levels of complexity. In predicting the appropriate structure, a suitable choice of the number of hidden layers and the number of nodes in each layer, together with the type of activation function and training algorithm, is very important. Many methods have been proposed to determine suitable values for these purposes, ranging from indirect methods based on trial and error to those that use empirical or statistical information [25].

The ideal network, at the first place, balances the performance against the size. A network with too many neurons is prone to overfitting in which the learning algorithm fits the training set so well that noise and the abnormalities of the training data are memorized. As a result of this, the learning algorithm's performance drops when it is examined in an unknown dataset. On the other hand, a network with too few neurons will be unable to learn all the relationships in the data, so its predictions will be unreliable [26].

In the next place, training in a back propagation algorithm is performed by forward and backward operation. Back-propagation is typically done on feed-forward neural networks and is able to generalize well on a wide variety of problems. The network

produces its actual outputs for a certain input pattern using current connection weights. Subsequently, the backward operation is carried out to alter the weights to decrease the error between the actual and desired outputs [27].

Lastly, the input value is passed through the neural network again with updated new weights, and the errors, if any, are calculated again. This technique is iterated until the error is acceptable (maximum 1000 epochs in this study). This method is continued for all the data in the training data. Finally, the test data are used to verify the nonlinear relationship between the input and output data sets.

A fact that fluorescent materials present difficulties for match prediction due to their variable excitation and emission characteristics caused that a few approaches have been investigated [28]. This work attempted to approximate the emission spectra of fluorescent materials from their absorbance using the principal component analysis technique and artificial neural networks. The performance of variety structure and topology of the network was evaluated by calculating root mean square (RMS) error.

2. Materials and methods

The emission spectra of fluorescent materials were reconstructed by using their absorbance spectra as follows:

– The absorbance and emission spectra of 34 fluorescent materials were measured at 20 nm intervals from 300 to 800 nm, and were available from [29].

– Principal component eigenvectors of absorbance and emission spectral data were calculated and divided into training (25 samples) and testing (9 samples) data set.

– Neural networks of different algorithms, namely cascade- and feed-forward networks, were applied to train the neural networks in order to predict the principal component eigenvectors of emission spectra. In this section, the effect of the neural networks parameters such as the number of hidden layers and the number of neurons per each layer on reconstruction accuracy was evaluated.

– Emission spectra of fluorescent materials were calculated using their predicted principal component eigenvectors.

– The performance of neural networks with various topologies and structures was evaluated using RMS error.

3. Principal component analysis

The PCA technique was applied to the absorption and emission spectra of 34 fluorescent materials. The output of a PCA consists of a series of eigenvalues and eigenvectors (each eigenvalue corresponding to an eigenvector).

Figure 1 represents the principal component eigenvalues of absorption and emission spectra. Eigenvalues can be thought of as quantitative assessment of how much a component represents the data. The higher the eigenvalues of a component, the more representative it is of the data. The optimal number of eigenvectors depends on the application and accuracy requirement. It is clear that the total variance of reflectance spectra could be explained by first four principal components whereas the rest are insignificant.

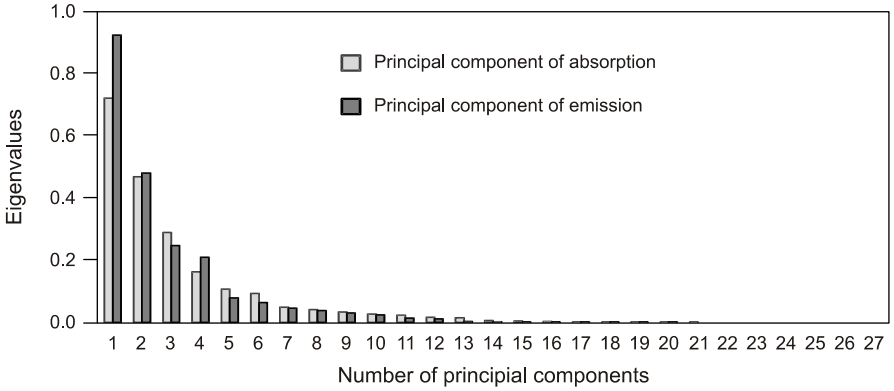

Fig. 1. Principal components eigenvalues of absorption and emission samples.

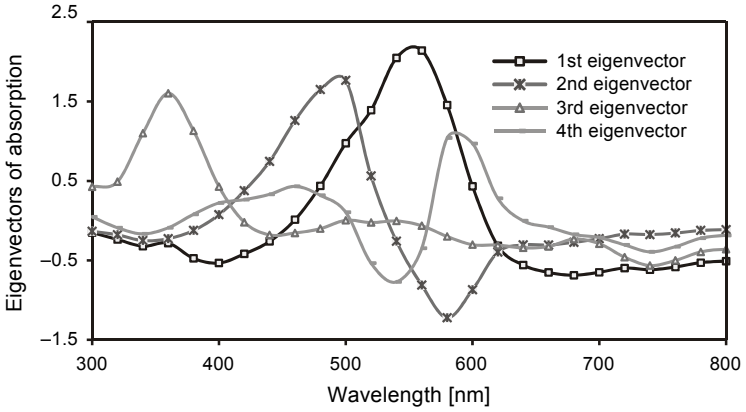

Fig. 2. The first four eigenvectors of principal components of absorption.

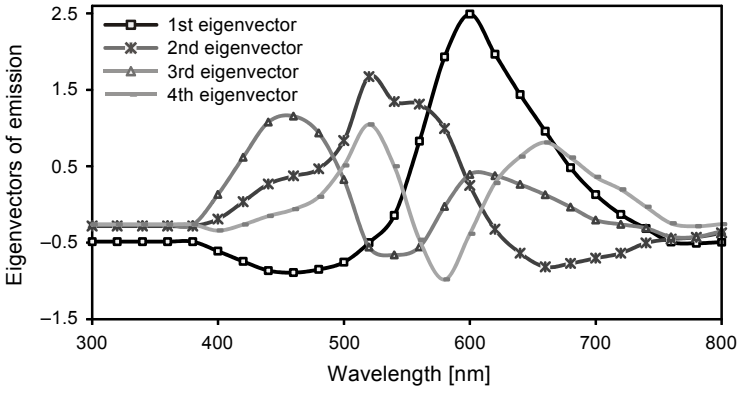

Fig. 3. The first four eigenvectors of principal components of emission.

Eigenvectors, on the other hand, can be thought of as "preferential directions" of a data set, or in other words, main patterns in the data. The first four eigenvectors of absorption and emission spectra are illustrated in Figs. 3 and 4, respectively. Each eigenvector corresponds to one of the eigenvalues and associated principal components and is used to form linear combinations of the variables.

4. Neural network predictive model

The feed- and cascade-forward neural networks consisting of two and three hidden layers were utilized to make the relationship between first four principal components of absorbance, which served as inputs to the network, and first four principal components of emission that were designated as outputs of the network.

Feed-forward networks (Fig. 4**a**) often have one or more hidden layers. The hidden layer consisted of sigmoid activation functions

$$\Phi(v) = \frac{1}{1 + \exp(-av)} \tag{2}$$

where a is the slope parameter of the sigmoid activation function. The output layers consisted of neurons with linear activation functions

$$\Phi(v) = v \tag{3}$$

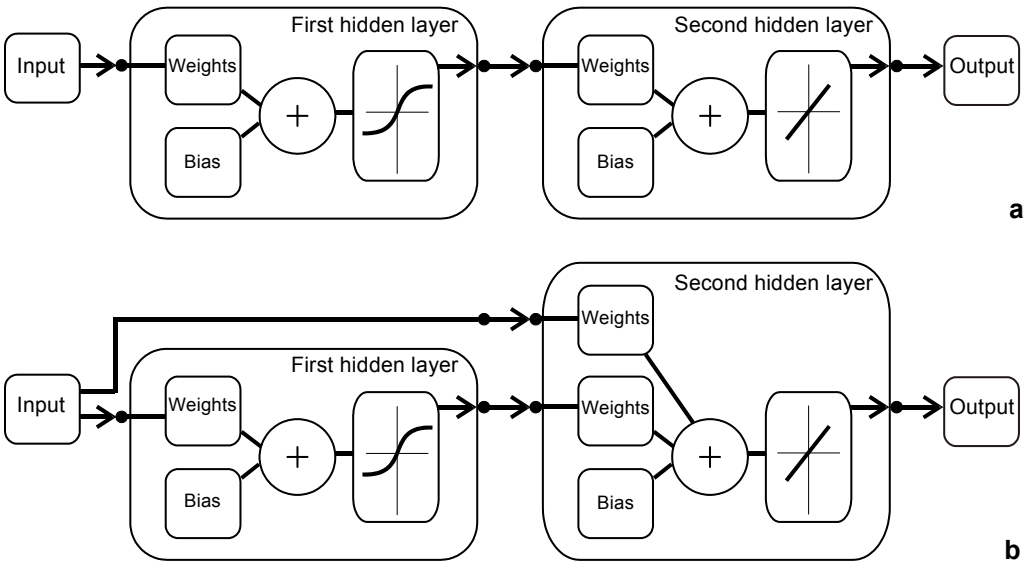

Fig. 4. A two-layer feed-forward (**a**) and cascade-forward (**b**) neural network structure of sigmoid neurons followed by an output layer of linear neurons.

Multiple layers of neurons with nonlinear transfer functions allow the network to learn nonlinear and linear relationships between input and output vectors.

Cascade-forward networks consist of n hidden layers (Fig. 4**b**), the first layer has weights coming from the input. Each subsequent layer has weights coming from the input and all previous layers. All layers have biases and the last layer is the network output.

The precision and predictive abilities of training and testing data sets were compared by means of RMS error, defined as

$$\text{RMS error} = \sqrt{\frac{\sum \Delta R_\lambda^2}{n}} \tag{4}$$

where ΔR_λ is the difference between the actual and reconstructed reflectance spectra at a certain wavelength λ and n represents the number of wavelengths in which measurements have been carried out.

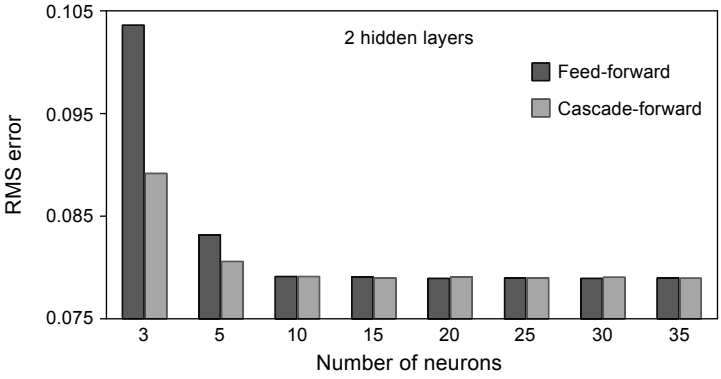

Fig. 5. Spectrophotometric accuracy of reconstructed training data set of emission spectra with (9 1) network structure, based on RMS error.

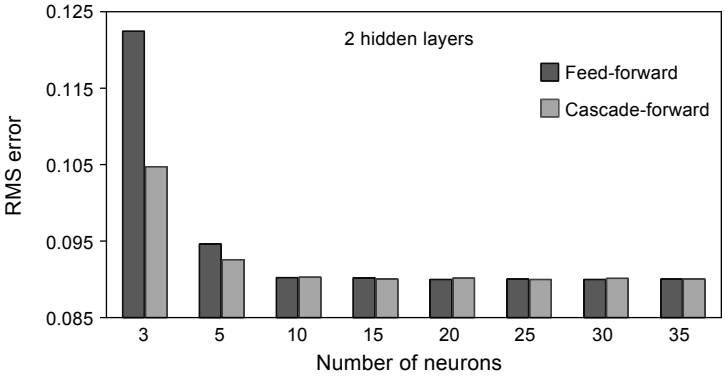

Fig. 6. Spectrophotometric accuracy of reconstructed testing data set of emission spectra with (9 1) network structure, based on RMS error.

Figures 5and 6 summarize the RMS error calculated for neural networks with two hidden layers and different numbers of neurons for training and testing data sets, respectively. Comparison of the results presented in Figs. 5 and 6 reveals that, increasing the number of neurons from 3 to 10, results in substantial reduction in RMS error and then the charts reach a plateau. As can be seen in Figs. 5 and 6, in feed-forward networks by growing the number of neurons from 3 to 10, RMS error in a training data set decreases from 0.104 to 0.079, and from 0.122 to 0.090 in a testing data set. Turning to cascade-forward networks, the same increase in the number of neurons results in declining of RMS error from 0.089 to 0.079 in a training data set and from 0.105 to 0.090 in a testing data set. Additionally, a further increase in the number of neurons has a marginal effect on network performance.

Same trend can be seen from the networks with three hidden layers. Regarding Figs. 7 and 8, with increasing the number of neurons from 3 to 10, RMS error represents a downward trend from 0.141 to 0.083 for reconstructed data obtained from feed-forward networks in a training data set (Fig. 7), and from 0.165 to 0.094 in a testing data

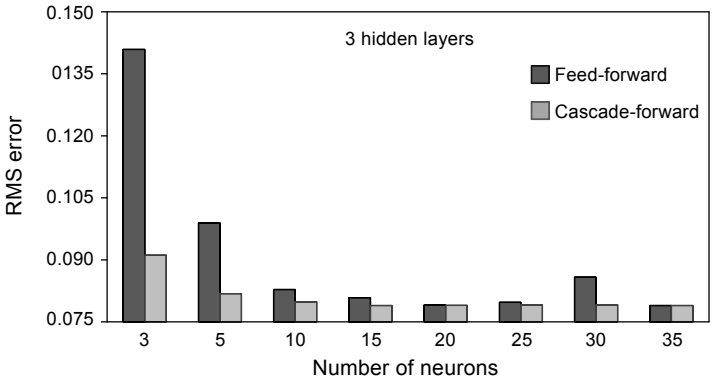

Fig. 7. Spectrophotometric accuracy of reconstructed training data set of emission spectra with (4 5 1) network structure, based on RMS error.

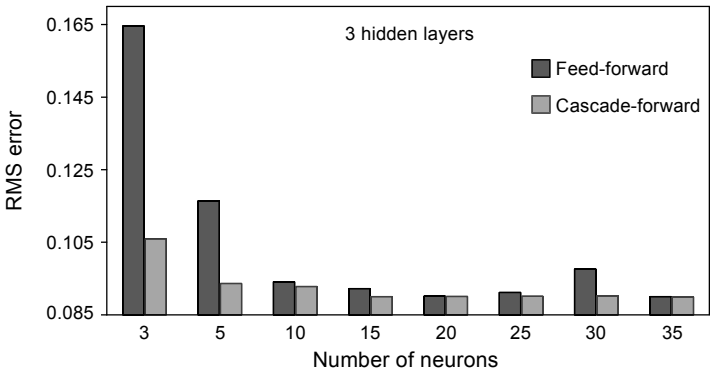

Fig. 8. Spectrophotometric accuracy of reconstructed testing data set of emission spectra with (4 5 1) network structure, based on RMS error.

set (Fig. 8). Likewise, in cascade-forward networks, RMS error falls from 0.091 to 0.090 in a training data set and from 0.106 to 0.093 in a testing data set.

To sum up Figs. 5 to 8, in most cases it can be deduced that cascade-forward neural networks exhibit better performance in comparison with feed-forward neural networks in both training and testing data sets, especially in small numbers of neurons. Furthermore, increasing the number of hidden layers from two hidden layers to three hidden layers leads to an increase in RMS error and also results in some degree of network instability.

In this study, the maximum and minimum RMS errors were 0.1646 and 0.08993 for feed- and cascade-forward neural networks with three hidden layers, respectively.

The neural network with two hidden layers and ten neurons has been selected as an optimum structure for both cascade- and feed-forward neural networks. Figures 9 and 10 represent typical reconstructed spectra using neural networks with 3 and 10 neurons and two hidden layers, respectively, in comparison with actual spectra. It is seen

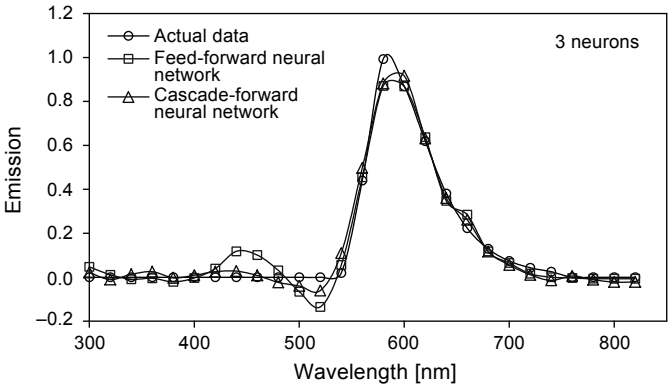

Fig. 9. Actual and predicted emission spectra of sample with (2 1) network structure.

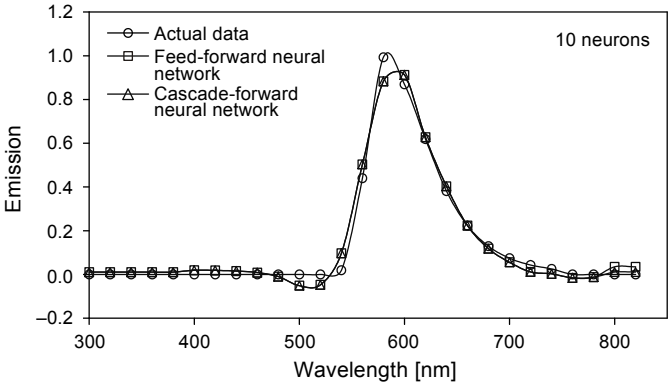

Fig. 10. Actual and predicted emission spectra of sample with (9 1) network structure.

in the figure that increasing the number of neurons from 3 to 10 improved the performance of both networks.

A fluorophore absorbs energy of a specific wavelength $\lambda_{\text{max-ex}}$ and then re-remits the energy at a different but equally specific wavelength $\lambda_{\text{max-em}}$, therefore $\lambda_{\text{max-ex}}$ and $\lambda_{\text{max-em}}$ are two characteristics of fluorescent spectra. Figures 11 and 12 show the correlation between the actual $\lambda_{\text{max-em}}$ and those obtained from the cascade- and feed-forward networks with two hidden layers, respectively. The least-square regression lines are given by the average prediction vector $\lambda_{p(i)}$ equal to $0.989x$ and $0.987x$ for (2H, 10N) cascade- and feed-forward neural networks, respectively. On the other hand, with respect to Figs. 13 and 14, those which correspond to (3H, 10N) cascade- and feed-forward neural networks are equal to $0.986x$ and $0.985x$, respectively. This indicates a strong agreement between the actual data and the predicted results.

An important aspect of correlation is how strong it is. The strength of a correlation is measured by the correlation coefficient r or the Pearson product moment correlation coefficient. The correlation coefficients between the actual $\lambda_{\text{max-em}}$ and the predicted results λ_p are given by

$$\Delta\lambda_{\text{max-em}} = \sqrt{1 - \frac{\sum_{i=1}^{N} (\lambda_{(i)} - \lambda_{p(i)})^2}{\sum_{i=1}^{N} (\lambda_{(i)} - \overline{\lambda})^2}} \tag{5}$$

where $\overline{\lambda}$ is the mean of the actual $\lambda_{\text{max-em}}$ vector and N is the size of the available dataset [30].

With respect to Figs. 11–14, the correlation coefficients of all four neural network architectures were more than 0.97, which indicates that these variables can be considered as highly correlated. Moreover, cascade-forward back-propagation neural networks with two hidden layers had the highest correlation coefficient among the others.

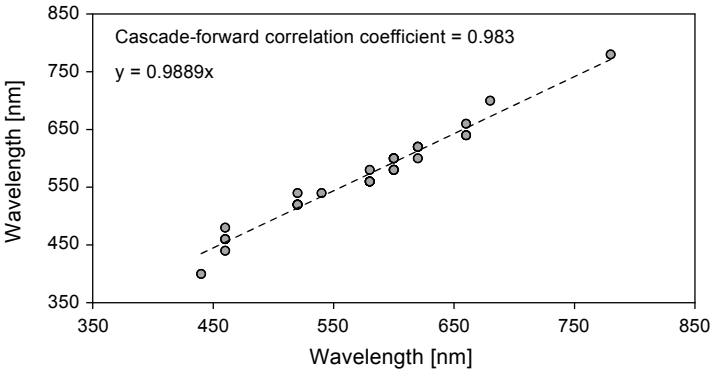

Fig. 11. Correlation between actual data and predicted maximum emission wavelength λ_{max} obtained from cascade-forward (9 1) network structure.

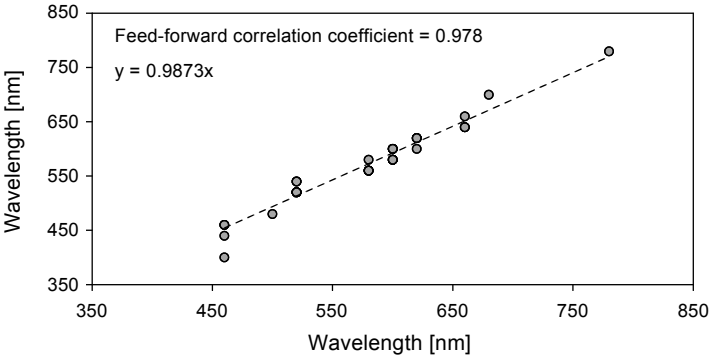

Fig. 12. Correlation between actual data and predicted maximum emission wavelength λ_{max} obtained from feed-forward (9 1) network structure.

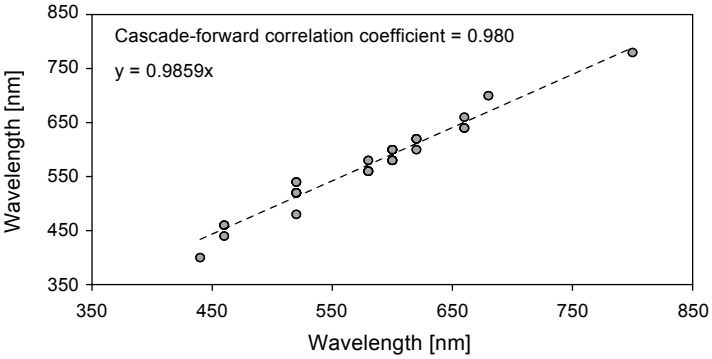

Fig. 13. Correlation between actual data and predicted maximum emission wavelength λ_{max} obtained from cascade-forward (4 5 1) network structure.

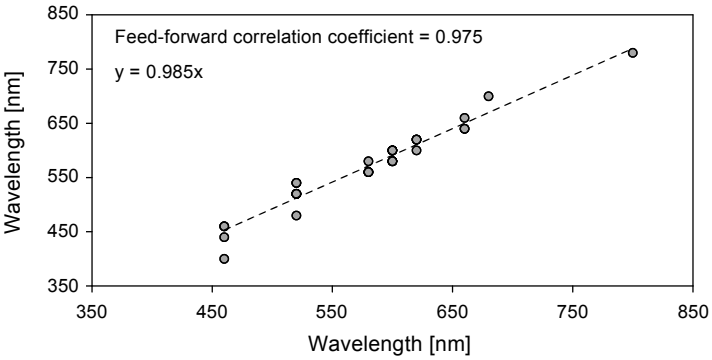

Fig. 14. Correlation between actual data and predicted maximum emission wavelength λ_{max} obtained from feed-forward (4 5 1) network structure.

T a b l e 1. Calculated difference between actual $\lambda_{max\text{-}em}$ and the predicted results.

Neural network structure		Mean [nm]	Max [nm]	Min [nm]	SD
Cascade-forward algorithm	2 hidden layers with (9 1)	10.0	40	0	11.3
	3 hidden layers with (4 5 1)	11.8	40	0	12.2
Feed-forward algorithm	2 hidden layers with (9 1)	11.2	60	0	13.2
	3 hidden layers with (4 5 1)	12.4	60	0	13.9

Table 1 represents the deviation of the outputs obtained from networks with selected structures from the actual $\lambda_{max\text{-}em}$ values. With respect to Table 1, the mean deviation from the actual values varies from 10 to 12.4 for cascade-forward networks with (9 1) structures and feed-forward networks with (4 5 1) structures, respectively, which confirms preceding results.

5. Conclusion

Because of simplicity and the ability to carry out detailed analysis, neural networks based on the back-propagation algorithm with different topologies were used to distinguish the first four principal components of emission from those of absorbance.

The analysis of the relationship between the predicted results of the designed artificial neural network model and the experimental data was also conducted. According to obtained results from all the structures, RMS error was situated at the 0.1646–0.0899 interval. In addition, neural networks with two hidden layers and 10 neurons have been selected as optimum structure for both cascade- and feed-forward neural networks. As well, the simulated results showed high correlation between the actual and predicted maximum absorption wavelength. According to obtained results, correlation coefficients of all architectures were more than 0.97, which indicates that these variables can be considered as highly correlated.

Depending on these observations, the neural network approach can be considered as a promising tool for predicting the emission spectra of fluorescent materials.

References

[1] Seong-il Um, Yonghan Kang, Joon-Kyun Lee, *The synthesis and properties of triazine-stilbene fluorescent brighteners containing a monophenolic antioxidant*, Dyes and Pigments **75**(3), 2007, pp. 681–686.

[2] Christie R.M., Morgan K.M., Saiful Islam M., *Molecular design and synthesis of N-arylsulfonated coumarin fluorescent dyes and their application to textiles*, Dyes and Pigments **76**(3), 2008, pp. 741–747.

[3] Staneva D., Grabchev I., Betcheva R., *Sensor potential of 1,8-naphthalimide and its dyeing ability of cotton fabric*, Dyes and Pigments **98**(1), 2013, pp. 64–70.

[4] Kaur B., Bhattacharya S.N., Henry D.J., *Interpreting the near-infrared reflectance of a series of perylene pigments*, Dyes and Pigments **99**(2), 2013, pp. 502–511.

[5] GOMES E.C.C., DE CARVALHO I.M.M., DIÓGENES I.C.N., DE SOUSA E.H.S., LONGHINOTTI E., *On the incorporation of Rhodamine B and 2',7'-dichlorofluorescein dyes in silica: synthesis of fluorescent nanoparticles*, Optical Materials **36**(7), 2014, pp. 1197–1202.
[6] MARKOVA L.I., TERPETSCHNIG E.A., PATSENKER L.D., *Comparison of a series of hydrophilic squaraine and cyanine dyes for use as biological labels*, Dyes and Pigments **99**(3), 2013, pp. 561–570.
[7] SAUER M., HOFKENS J., ENDERLEIN J., *Handbook of Fluorescence Spectroscopy and Imaging: From Ensemble to Single Molecules*, Wiley-VCH, Weinheim, 2011.
[8] LAKOWICZ J.R., *Principles of Fluorescence Spectroscopy*, 3rd Ed., Springer US, 2006.
[9] SATAM M.A., RAUT R.K., SEKAR N., *Fluorescent azo disperse dyes from 3-(1,3-benzothiazol-2-yl)-naphthalen-2-ol and comparison with 2-naphthol analogs*, Dyes and Pigments **96**(1), 2013, pp. 92–103.
[10] AIFENG LIU, LIANG YANG, ZHENYU ZHANG, ZHILAN ZHANG, DONGMEI XU, *A novel rhodamine-based colorimetric and fluorescent sensor for the dual-channel detection of Cu^{2+} and Fe^{3+} in aqueous solutions*, Dyes and Pigments **99**(2), 2013, pp. 472–479.
[11] DIBYENDU DEY, JABA SAHA, ARPAN DATTA ROY, BHATTACHARJEE D., SYED ARSHAD HUSSAIN, *Development of an ion-sensor using fluorescence resonance energy transfer*, Sensors and Actuators B: Chemical **195**, 2014, pp. 382–388.
[12] OOYAMA Y., SHIMADA Y., KAGAWA Y., YAMADA Y., IMAE I., KOMAGUCHI K., HARIMA Y., *Synthesis of new-type donor-acceptor π-conjugated benzofuro[2,3-c]oxazolo[4,5-a]carbazole fluorescent dyes and their photovoltaic performances of dye-sensitized solar cells*, Tetrahedron Letters **48**(52), 2007, pp. 9167–9170.
[13] KOZMA E., CATELLANI M., *Perylene diimides based materials for organic solar cells*, Dyes and Pigments **98**(1), 2013, pp. 160–179.
[14] SHUCAI LIANG, YANBIN LIU, JIN XIANG, MENG QIN, HUI YU, GUOPING YAN, *Fabrication of a new fluorescent polymeric nanoparticle containing naphthalimide and investigation on its interaction with bovine serum albumin*, Colloids and Surfaces B: Biointerfaces **116**, 2014, pp. 206–210.
[15] BETTATI S., PASQUALETTO E., LOLLI G., CAMPANINI B., BATTISTUTTA R., *Structure and single crystal spectroscopy of Green Fluorescent Proteins*, Biochimica et Biophysica Acta (BBA) – Proteins and Proteomics **1814**(6), 2011, pp. 824–833.
[16] WOLD S., ESBENSEN K., GELADI P., *Principal component analysis*, Chemometrics and Intelligent Laboratory Systems **2**(1–3), 1987, pp. 37–52.
[17] WESTLAND S., RIPAMONTI C., *Computational Colour Science Using MATLAB*, John Wiley & Sons, 2004.
[18] VEIT D., *Neural networks and their application to textile technology*, [In] *Simulation in Textile Technology*, 1st Ed., Woodhead Publishing Limited, 2012, pp. 9–71.
[19] RUEY-FANG YU, CHUANG-HUNG LIN, HO-WEN CHEN, WEN-PO CHENG, MING-CHIEN KAO, *Possible control approaches of the Electro-Fenton process for textile wastewater treatment using on-line monitoring of DO and ORP*, Chemical Engineering Journal **218**, 2013, pp. 341–349.
[20] KUMAR A., *Neural network based detection of local textile defects*, Pattern Recognition **36**(7), 2003, pp. 1645–1659.
[21] STANIKUNAS R., VAITKEVICIUS H., KULIKOWSKI J.J., *Investigation of color constancy with a neural network*, Neural Networks **17**(3), 2004, pp. 327–337.
[22] KAYDANI H., MOHEBBI A., *A comparison study of u sing optimization algorithms and artificial neural networks for predicting permeability*, Journal of Petroleum Science and Engineering **112**, 2013, pp. 17–23.
[23] ADDEH J., EBRAHIMZADEH A., AZARBAD M., RANAEE V., *Statistical process control using optimized neural networks: a case study*, ISA Transactions **53**(5), 2014, pp. 1489–1499.
[24] FENG LUAN, XUAN XU, HUITAO LIU, DIAS SOEIRO CORDEIRO M.N., *Review of quantitative structure-activity/property relationship studies of dyes: recent advances and perspectives*, Coloration Technology **129**(3), 2013, pp. 173–186.

[25] CURTEANU S., CARTWRIGHT H., *Neural networks applied in chemistry. I. Determination of the optimal topology of multilayer perceptron neural networks*, Journal of Chemometrics **25**(10), 2011, pp. 527–549.
[26] TETKO I.V., LIVINGSTONE D.J., LUIK A.I., *Neural network studies. 1. Comparison of overfitting and overtraining*, Journal of Chemical Information and Modeling **35**(5), 1995, pp. 826–833.
[27] KOKER R., ALTINKOK N., DEMIR A., *Neural network based prediction of mechanical properties of particulate reinforced metal matrix composites using various training algorithms*, Materials and Design **28**(2), 2007, pp. 616–627.
[28] DE M BEZERRA C., HAWKYARD C.J., *Computer match prediction for fluorescent dyes by neural networks*, Coloration Technology **116**(5–6), 2000, pp. 163–169.
[29] www.tsienlab.ucsd.edu/Documents/REF%20-%20Fluorophore%20Spectra.xls
[30] SARKAR K., MOUNIR BEN GHALIA, ZHENHUA WU, BOSE S.C., *A neural network model for the numerical prediction of the diameter of electro-spun polyethylene oxide nanofibers*, Journal of Materials Processing Technology **209**(7), 2009, pp. 3156–3165.

Received April 26, 2014